Smart Structures and Systems, *Vol. 12, No. 3-4 (2013) 363-379*
DOI:http://dx.doi.org/10.12989/sss.2013.12.3_4.363

A vision-based system for dynamic displacement measurement of long-span bridges: algorithm and verification

X.W. Ye[1,2], Y.Q. Ni[*1], T.T. Wai[1], K.Y. Wong[3], X.M. Zhang[4] and F. Xu[1]

[1]Department of Civil and Environmental Engineering, The Hong Kong Polytechnic University, Hung Hom, Kowloon, Hong Kong
[2]Department of Civil Engineering, Zhejiang University, Hangzhou 310058, China
[3]Highways Department, The Hong Kong SAR Government, Hong Kong
[4]Intelligent Structural Health Monitoring R&D Centre, The Hong Kong Polytechnic University Shenzhen Research Institute, Shenzhen 518057, China

(Received January 12, 2013, Revised February 5, 2013, Accepted February 15, 2013)

Abstract. Dynamic displacement of structures is an important index for in-service structural condition and behavior assessment, but accurate measurement of structural displacement for large-scale civil structures such as long-span bridges still remains as a challenging task. In this paper, a vision-based dynamic displacement measurement system with the use of digital image processing technology is developed, which is featured by its distinctive characteristics in non-contact, long-distance, and high-precision structural displacement measurement. The hardware of this system is mainly composed of a high-resolution industrial CCD (charge-coupled-device) digital camera and an extended-range zoom lens. Through continuously tracing and identifying a target on the structure, the structural displacement is derived through cross-correlation analysis between the predefined pattern and the captured digital images with the aid of a pattern matching algorithm. To validate the developed system, MTS tests of sinusoidal motions under different vibration frequencies and amplitudes and shaking table tests with different excitations (the El-Centro earthquake wave and a sinusoidal motion) are carried out. Additionally, in-situ verification experiments are performed to measure the mid-span vertical displacement of the suspension Tsing Ma Bridge in the operational condition and the cable-stayed Stonecutters Bridge during loading tests. The obtained results show that the developed system exhibits an excellent capability in real-time measurement of structural displacement and can serve as a good complement to the traditional sensors.

Keywords: vision-based system; displacement measurement; digital image processing; pattern matching algorithm; cable-supported bridge; experimental verification

1. Introduction

Structural health monitoring (SHM) has been a cutting-edge technology and gained increasing concerns worldwide, especially in the civil engineering community (Stull *et al*. 2012). A lot of newly constructed large-scale civil structures have been instrumented with long-term SHM systems (Wong 2004, Ko and Ni 2005, Ni *et al*. 2009, Kim and Laman 2012). Design and

*Corresponding author, Professor, E-mail: ceyqni@polyu.edu.hk

http://www.techno-press.org/?journal=sss&subpage=8 ISSN: 1738-1584 (Print), 1738-1991 (Online)

implementation of such a system is primarily aimed to continuously monitor the environmental and operational loads imposed on the structure as well as the structural features and responses through deploying various types of traditional and innovative sensors, and subsequently to assess/evaluate the structural health/safety condition and identify/locate the structural damage with the aid of intelligent data processing methodologies (Okasha and Frangopol 2012). For long-span bridges and high-rise buildings, the dynamic displacement of the structures under operational conditions is an important indicator of structural behavior and health status; while accurate measurement of structural displacement for such structures is still a challenge (Wahbeh *et al.* 2003, Chang and Ji 2007, Choi *et al.* 2011).

Considerable research efforts have been devoted to the development of structural displacement measurement techniques which are mainly referred to two kinds with the use of contact transducers and non-contact sensors, respectively. For the contact transducers, the linear variable differential transformer (LVDT) has been the most widely used sensor for structural displacement measurement. This kind of sensor, however, needs a stationary reference platform which is not easily achieved for large-scale structures and when the structure is inaccessible or prohibited to be approached (Fukuda *et al.* 2010). Alternatively, extensive investigations have been conducted on indirect structural displacement measurement through double integration of recorded acceleration data with appropriate filter selection and baseline correction (Park *et al.* 2005), or derivation from the strain-deflection relationship based on measured strain time histories (Kim and Cho 2004); while the accuracy is limited.

Non-contact type displacement measurement techniques mainly include the global positioning system (GPS) and the laser Doppler vibrometer (LDV). A significant number of studies have been carried out on GPS-based structural displacement measurement, for recent examples, Yi *et al.* (2011, 2013) conducted extensive research on the characterization and extraction of GPS multipath signals and the performance assessment of high-rate GPS receivers. An insight into most of the available literature reveals that the GPS enables real-time structural displacement measurement with millimeter-level accuracy at a frequency up to 20 Hz (Xu *et al.* 2002, Yi *et al.* 2012). However, the measurement instruments are quite costly, especially when the structural displacements at a large number of locations are desired to be synchronously measured. On the other hand, the LDV is capable of providing accurate multiple-location structural displacement measurement in a certain distance; yet the devices are also expensive and the laser intensity may become dangerously strong in some occasions (Nassif *et al.* 2005, Lee and Shinozuka 2006).

With the rapid progress of photonics science and image processing technology, vision-based monitoring systems have been developed and offered as an effective alternative for structural displacement measurement. The research and applications of various vision-based structural displacement measurement systems have been reported in recent years. Jauregui *et al.* (2003) conducted a study of vertical deflection measurement of bridges by use of digital close-range terrestrial photogrammetry (DCRTP), and satisfactory results were obtained in laboratory and field experiments. Jurjo *et al.* (2010) presented an experimental methodology for dynamic analysis of structures based on digital image acquisition and processing techniques. Laboratory tests were carried out to evaluate the efficiency, precision, and accuracy of the proposed method, and the achieved results were favorably compared with those obtained from theoretical analyses and conventional sensors. Zaurin and Catbas (2010) established a framework for condition assessment and performance evaluation of engineering structures by integrating video images with synchronized sensor measurements. Santos *et al.* (2012) proposed a calibration method for a vision-based displacement measurement system, and its reliability and robustness was validated

through numerical simulation experiments.

Although considerable work has been carried out on structural displacement measurement using machine vision technology, development of a non-contact, cost-effective, and real-time vision-based system with the distinct characteristics of long-distance and high-precision for displacement measurement of large-scale civil structures is still desirable. This paper presents a vision-based dynamic displacement measurement system which is composed of advanced optical devices and customized digital image data processing software. The performance of the developed system is verified through the laboratory MTS and shaking table tests as well as the field measurement of the mid-span vertical displacement of the suspension Tsing Ma Bridge in the operational condition and the cable-stayed Stonecutters Bridge during loading tests.

(a) (b) (c) (d)

Fig. 1 System hardware: (a) industrial CCD digital camera, (b) extended-range zoom lens, (c) laptop computer and (d) Gigabit Ethernet standard LAN wire

2. Vision-based dynamic displacement measurement system

2.1. System configuration

As illustrated in Fig. 1, the vision-based dynamic displacement measurement system comprises a high-resolution industrial CCD (charge-coupled-device) digital camera, an extended-range zoom lens, a laptop computer, and a Gigabit Ethernet standard LAN wire. The system measurement accuracy is dependent on the resolution of the CCD digital camera and the measurement distance between the digital camera and the target on the structure. In this system, a long-distance image acquisition device is developed by integrating the Prosilica GigE GC2450 camera with the Navitar 24X zoom extender lens, which is capable of visualizing the object in real time from a distance over one thousand meters. The resolution of the Prosilica GigE GC2450 camera is 2,456 pixels (horizontal) × 2,058 pixels (vertical). If the vertical movement range of the target is 400 mm with a measurement distance of 100 m away from the digital camera, the measurement accuracy is 400/2,058 = 0.194 mm/pixel in vertical direction; while the measurement accuracy is 2×400/2,058 = 0.389 mm/pixel in vertical direction when the target is distanced from the digital camera by 200 m. In the field structural displacement measurement, an LED lamp is usually fixed on the structure as the target when the structure is accessible; otherwise a feature point of the structure will be specified as an alternative target. Through recognizing and tracking the target on the structure, the dynamic displacement of the object structure is derived with the aid of the digital image processing technique. Fig. 2 shows the LabVIEW-based software interface of the developed

vision-based system for dynamic displacement measurement of bridge structures.

Fig. 2 LabVIEW-based system software interface

2.2. Pattern matching algorithm

Pattern matching is an effective means for digital image processing, which is able to promptly locate the target in an image that matches a predefined pattern (also called as a mask or a template). The pattern matching technique has been applied in diverse disciplines, such as determination of target position and orientation, measurement of object dimensions (length, diameter, angle, and other critical dimensions), flaw detection and inspection, and so forth. In the realization of the pattern matching technique, a pattern with identifiable target is firstly created and then it will be selected to match the subsequent image captured by the digital camera, and a score on the basis of the pattern matching algorithm will be calculated. When this score reaches the maximum value, it indicates that the pattern best corresponds with the target in the original image and meanwhile the target position is identified (Gonzalez and Woods 2008).

The normalized cross-correlation is one of the most popular pattern matching algorithms. As illustrated in Fig. 3, the correlation of a pattern $f(i, j)$ of size $m \times n$ with an image $g(x, y)$ of size $M \times N$ at the point (x, y) is expressed as

$$c = h(x, y) = \sum_{i=0}^{m-1} \sum_{j=0}^{n-1} f(i, j) g(x + i, y + j) \tag{1}$$

where $x = 0, 1, \ldots, M\text{-}1$; $y = 0, 1, \ldots, N\text{-}1$; $i = 0, 1, \ldots, m\text{-}1$; and $j = 0, 1, \ldots, n\text{-}1$.

Correlation computation is a process of moving the pattern $f(i, j)$ within the image area $g(x, y)$ and computing the value c in that area, which involves the sum of multiplying each pixel in the pattern by the image pixel that it overlaps. The maximum value of c indicates the position (x, y) where the pattern $f(i, j)$ best matches the image $g(x, y)$. However, the correlation function given in Eq. (1) has the disadvantage of being sensitive to scale changes of the pattern $f(i, j)$ and the image $g(x, y)$. In the present study, the normalized correlation coefficient, $\gamma(x, y)$ is used to perform pattern matching, which is defined as

$$\gamma(x,y)=\frac{\sum_{i=0}^{m-1}\sum_{j=0}^{n-1}\left[f(i,j)-\bar{f}\right]\left[g(x+i,y+j)-\bar{g}_{xy}\right]}{\left\{\sum_{i=0}^{m-1}\sum_{j=0}^{n-1}\left[f(i,j)-\bar{f}\right]^2\sum_{i=0}^{m-1}\sum_{j=0}^{n-1}\left[g(x+i,y+j)-\bar{g}_{xy}\right]^2\right\}^{\frac{1}{2}}} \tag{2}$$

where $\bar{f}$ is the average value of the pattern $f(i, j)$, and $\bar{g}_{xy}$ is the average value of the image $g(x, y)$ in the region coincident with the pattern $f(i, j)$.

It is known from Eq. (2) that the normalized correlation coefficient has values in the range [-1, 1], which is independent of the amplitude changes of the pattern $f(i, j)$ and the image $g(x, y)$. The maximum value of the normalized correlation coefficient occurs when the normalized pattern is identical with the corresponding normalized region in the image.

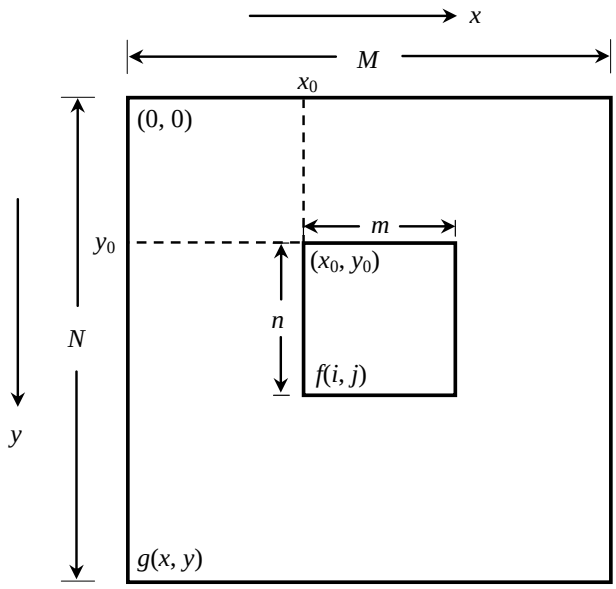

Fig. 3 Cross-correlation between pre-designated pattern and captured image

2.3. Target localization method

Fig. 4 shows the schematic chart of structural displacement measurement based on pattern matching. Firstly, the images containing the target on the structure are captured by the digital camera, and a pattern with initial pixel coordinates is extracted from the acquired image. Then, the process of pattern matching is continuously performed between the predefined pattern and the succeeding images captured by the digital camera. Making use of Eq. (2), the normalized correlation coefficients are calculated in the process of moving the pattern within the image area. The pixel coordinates of the target position will be obtained and retained once the normalized correlation coefficient reaches the maximum, indicating that the pattern best matches the image at

this location. Subsequently, the offset of the target in the pixel coordinate system is obtained by subtracting the pixel coordinates at the identified location with the initial pixel coordinates. Then the structural displacement is derived from the obtained coordinate offset and the scale ratio between the actual size of the pattern and the pixels of the pattern in the image. In the acquisition of displacement, only the target coordinates rather than the image signals need to be stored in the computer.

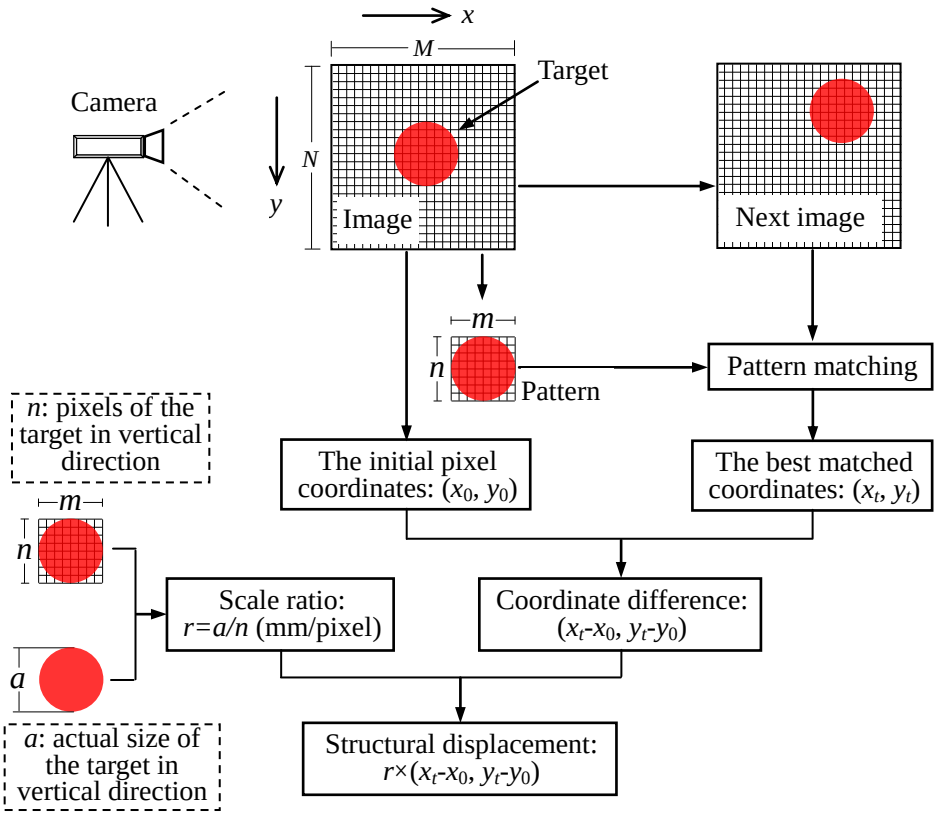

Fig. 4 Flowchart of vision-based structural displacement measurement

3. System performance evaluation by laboratory tests

3.1. MTS tests

To evaluate the feasibility and accuracy of the developed vision-based displacement measurement system, laboratory tests were firstly carried out using an MTS 810 material testing system. A target was attached on the base of the MTS and moved automatically in the vertical direction under different vibration amplitudes and frequencies. In this study, the distance between the target and the digital camera was set as 5 m. As illustrated in Fig. 5, two types of targets, i.e., LED lamp target and black dot target were used respectively for performance comparison of the

vision-based system in displacement measurement. The dynamic displacement of the target was synchronously measured by the MTS and the vision-based displacement measurement system with a sampling frequency of 25 Hz.

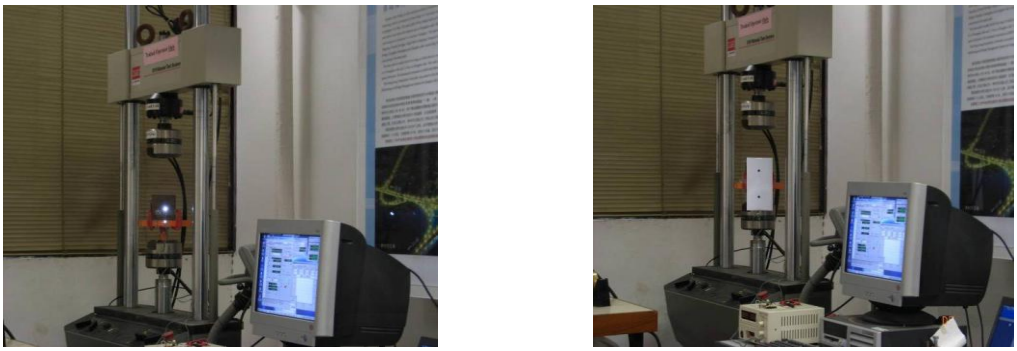

(a) LED lamp target (b) Black dot target

Fig. 5 Experimental setup of MTS tests

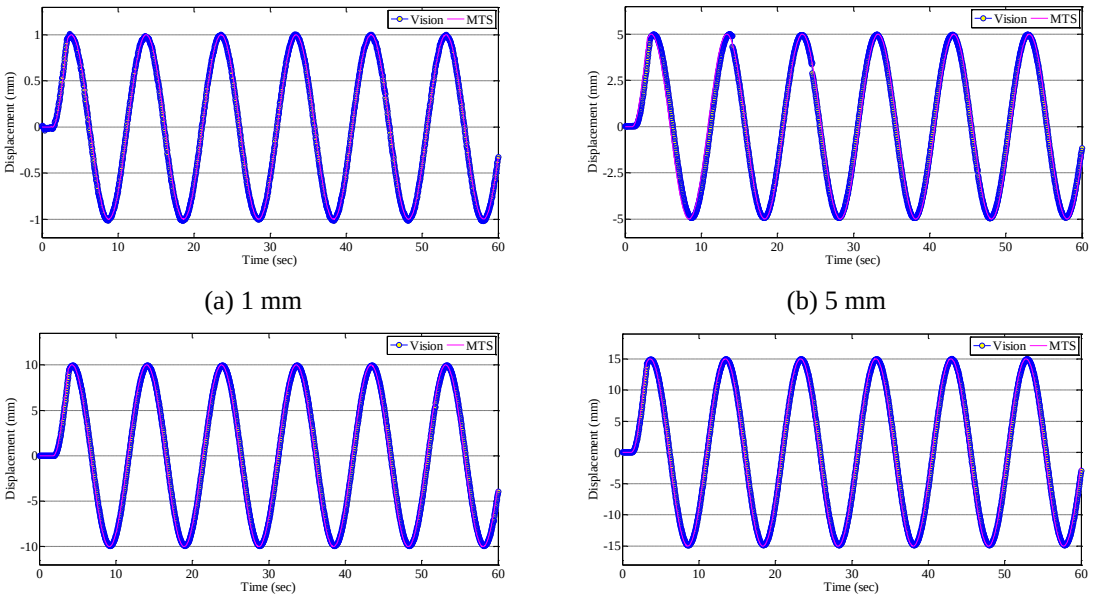

(a) 1 mm (b) 5 mm

(c) 10 mm (d) 15 mm

Fig. 6 Comparison of displacement output from vision-based system and from MTS at different vibration amplitudes (target: LED lamp; vibration frequency: 0.1 Hz)

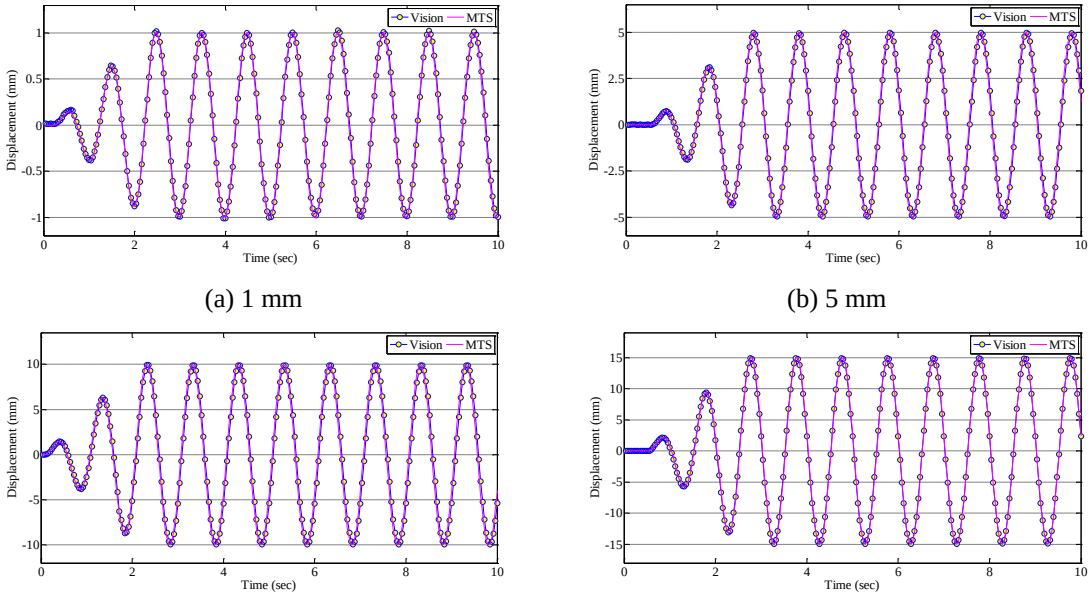

(a) 1 mm (b) 5 mm

(c) 10 mm (d) 15 mm

Fig. 7 Comparison of displacement output from vision-based system and from MTS at different vibration amplitudes (target: LED lamp; vibration frequency: 1 Hz)

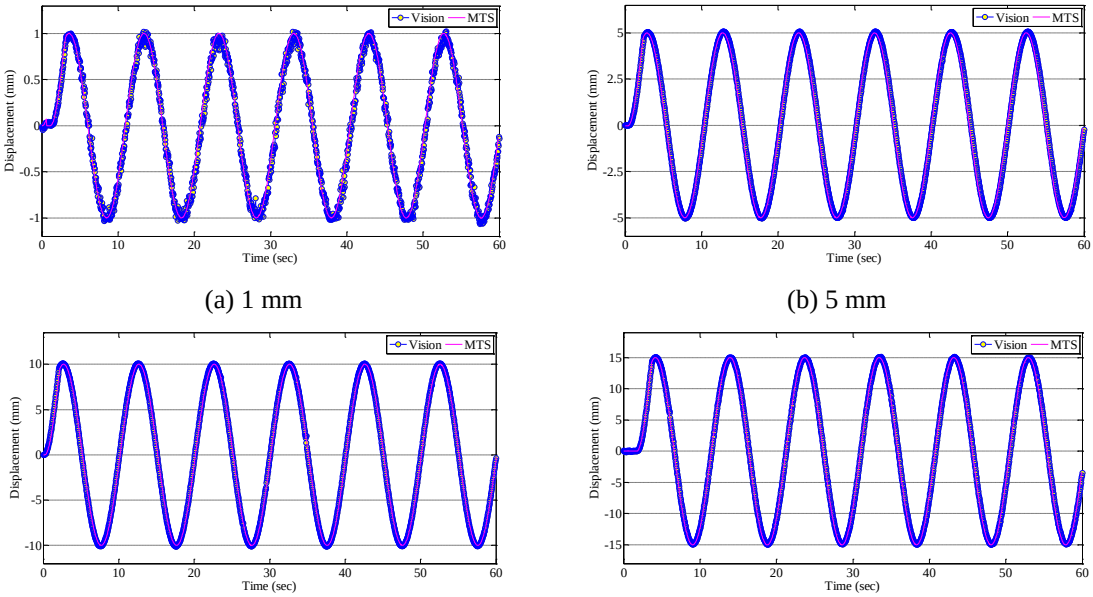

(a) 1 mm (b) 5 mm

(c) 10 mm (d) 15 mm

Fig. 8 Comparison of displacement output from vision-based system and from MTS at different vibration amplitudes (target: black dot; vibration frequency: 0.1 Hz)

Figs. 6 and 7 illustrate the displacement time histories of the LED lamp target in sinusoidal motions measured by the MTS and the vision-based system. In the sinusoidal excitation experiments, the LED lamp target was motivated at two vibration frequencies, namely, 0.1 Hz and 1 Hz with four different vibration amplitudes, namely, 1 mm, 5 mm, 10 mm, and 15 mm. It is seen from Figs. 6 and 7 that the output displacement results from the vision-based system are excellently coincident with those obtained by the MTS under different vibration frequencies and amplitudes. This observation indicates that the vision-based system has a good accuracy for dynamic displacement measurement when the distance between the system and the target is several meters.

With regard to field structural displacement measurement, the targeted structure is inaccessible in some occasions and the installation of the LED lamp target can be difficult and quite costly, if not impossible. In such cases, a feature point on the structure which is distinctive from its surrounding area will usually be extracted to be a tracing object. Figs. 8 and 9 show the measured displacement time histories of the black dot target by the MTS and the vision-based system. A good agreement is observed again between the displacement output from the MTS and that from the vision-based system.

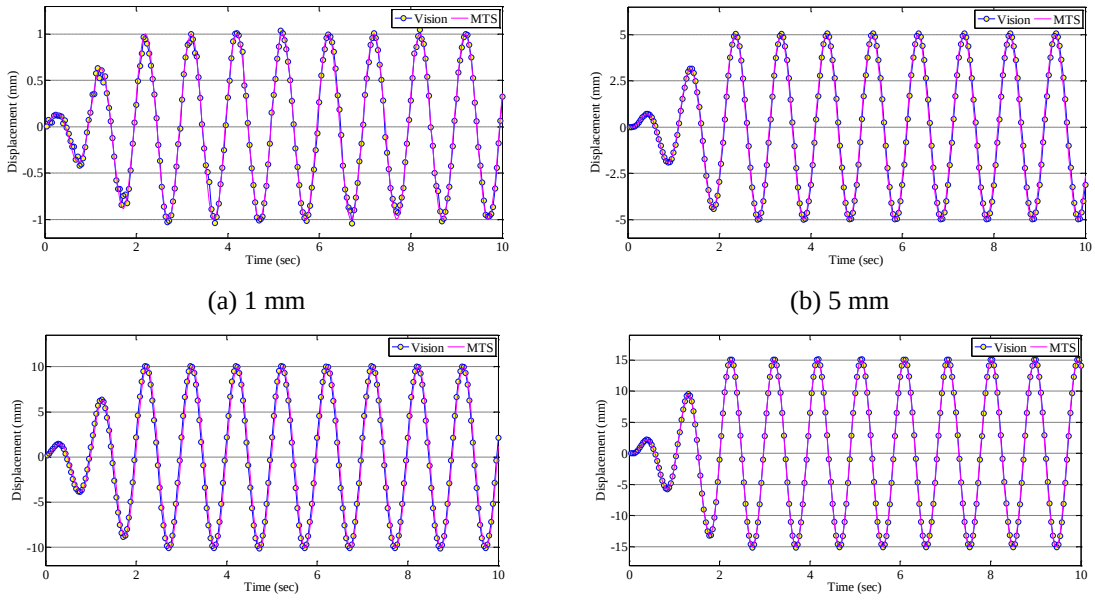

(a) 1 mm (b) 5 mm

(c) 10 mm (d) 15 mm

Fig. 9 Comparison of displacement output from vision-based system and from MTS at different vibration amplitudes (target: black dot; vibration frequency: 1 Hz)

Table 1 lists the obtained accuracy statistics of the developed vision-based system in reference to the MTS. The maximum difference, $d_{\max}$, the average difference, $\overline{d}$, and the root-mean-square error (RMSE) are calculated by

$$d_{\max} = \max\left(\left|d_i\right|\right) = \max\left(\left|V_i - M_i\right|\right) \tag{3}$$

$$\overline{d} = \frac{1}{n}\sum_{i=1}^{n}\left|d_i\right| = \frac{1}{n}\left[\left|V_1 - M_1\right| + \left|V_2 - M_2\right| + \cdots + \left|V_n - M_n\right|\right] \tag{4}$$

$$\mathrm{RMSE} = \sqrt{\frac{\sum_{i=1}^{n}\left(V_i - M_i\right)^2}{n}} \tag{5}$$

where V_i is the measured displacement by the vision-based system, M_i is the observed displacement by the MTS.

Table 1 Accuracy statistics of vision-based displacement measurement system

Target type	Vibration frequency (Hz)	Vibration amplitude (mm)	Maximum difference, $d_{\max}$ (mm)	Average difference, $\overline{d}$ (mm)	RMSE (mm)
LED lamp	0.1	1	0.0817	0.0247	0.0305
		5	1.2268	0.3820	0.4725
		10	1.0869	0.5258	0.5991
		15	1.3526	0.6853	0.7788
	1	1	0.1197	0.0091	0.0522
		5	0.6307	0.2400	0.3274
		10	1.6290	0.3504	0.9127
		15	0.6981	0.5926	0.3027
Black dot	0.1	1	0.2361	0.0602	0.0761
		5	0.6664	0.2875	0.3296
		10	0.7116	0.2688	0.3113
		15	1.0678	0.3914	0.4567
	1	1	0.2215	0.0400	0.0526
		5	0.5887	0.2539	0.3010
		10	1.4980	0.7525	0.8595
		15	0.9356	0.2961	0.3837

3.2. Shaking table tests

Shaking table tests were carried out to further verify the performance and stability of the developed vision-based displacement measurement system. As illustrated in Fig. 10, an LED lamp was fixed at the top plate of a single-story steel frame model installed on the shaking table. The vision-based system was placed on the ground 15 m away from the LED lamp target. In the present study, the shaking table was programmed to move under two different excitations, i.e., the El-Centro earthquake wave and a sinusoidal motion of 0.9 Hz. The horizontal displacement responses of the tested model were measured by the vision-based displacement measurement system at a sampling frequency of 20 Hz. Meanwhile, the displacement of the tested model was

simultaneously measured by a laser transducer for comparison. Figs. 11 and 12 illustrate the displacement responses of the tested model measured by the vision-based system and the laser transducer under the two excitations (the El-Centro earthquake wave and the sinusoidal motion). It is seen that the displacement responses measured by the vision-based system are in good agreement with those measured by the laser transducer in both the time and frequency domains.

Fig. 10 Experimental setup of shaking table tests

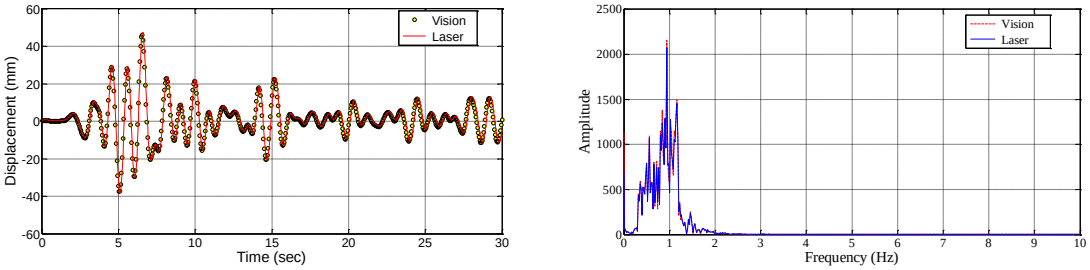

(a) Time domain (b) Frequency domain

Fig. 11 Comparison of displacement responses measured by vision-based system and laser transducer (El-Centro earthquake wave)

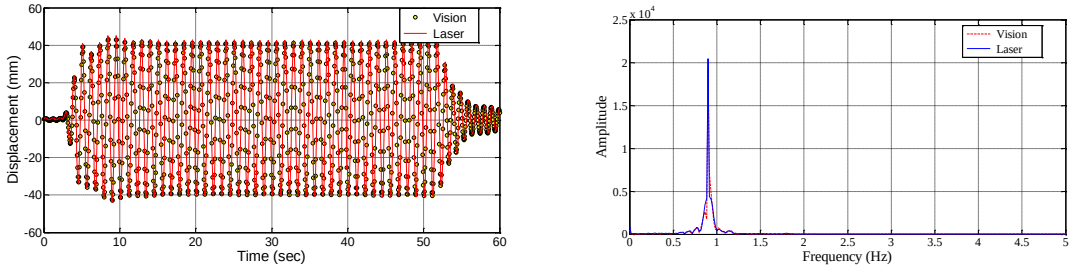

(a) Time domain (b) Frequency domain

Fig. 12 Comparison of displacement responses measured by vision-based system and laser transducer (sinusoidal motion of 0.9 Hz)

4. Field verification experiments

4.1. Displacement measurement of Tsing Ma Bridge at mid-span

The Tsing Ma Bridge in Hong Kong, as shown in Fig. 13, is a suspension bridge with a main span of 1,377 m and an overall length of 2,160 m. It carries a dual three-lane highway on its upper level of the bridge deck while two railway tracks and twin single-lane sheltered carriageways are located on the lower level of the bridge deck. As a combined highway and railway transport connection between the Tsing Yi Island and the Lantau Island, it forms a key part of the most essential transportation network linking the Hong Kong International Airport to the urban areas.

In the present study, the vision-based system was used to measure the vertical displacement of the Tsing Ma Bridge at mid-span with the purpose to examine its applicability for long-distance displacement measurement. As illustrated in Fig. 13, the digital camera was placed at the location approximately 1,000 m away from the mid-span of the Tsing Ma Bridge. As shown in Fig. 14, an LED lamp target was attached on a deck parapet adjacent to a GPS receiver which has been installed on the Tsing Ma Bridge as a part of the long-term SHM system implemented by the Highways Department of the Hong Kong Special Administrative Region Government (Wong 2007).

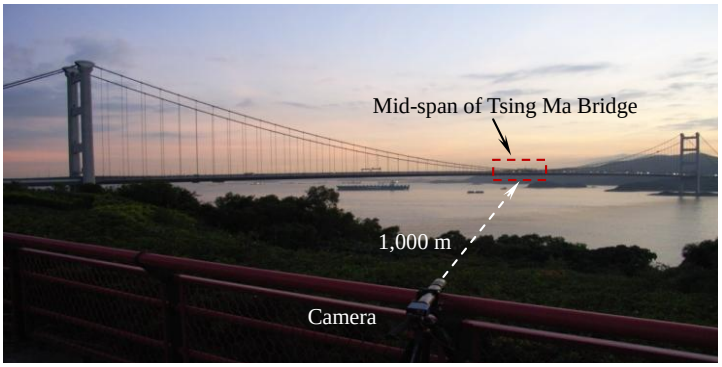

Fig. 13 Vision-based displacement measurement of Tsing Ma Bridge

Fig. 14 LED lamp target and GPS receiver installed on Tsing Ma Bridge

Fig. 15 shows the vertical displacement responses of the Tsing Ma Bridge at mid-span measured by the vision-based system and the GPS at a sampling frequency of 10 Hz. It is observed that the displacement responses measured by the vision-based system agree fairly well with those measured by the GPS in both the time and frequency domains. It is seen from Fig. 15(a) that the displacement pulses with large magnitudes appear in the displacement time history, which are mainly caused by train traffic. A further insight into Fig. 15(a) reveals that the maximum amplitude of the measured vertical displacement of the Tsing Ma Bridge at mid-span is 726.30 mm.

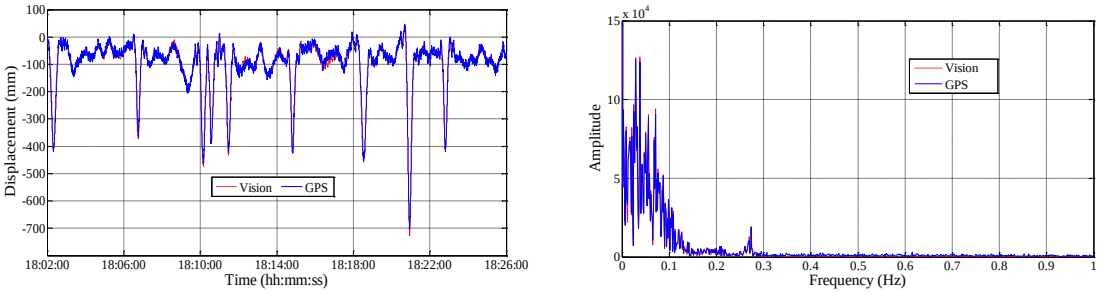

(a) Time domain (b) Frequency domain

Fig. 15 Comparison of displacement responses at mid-span measured by vision-based system and GPS

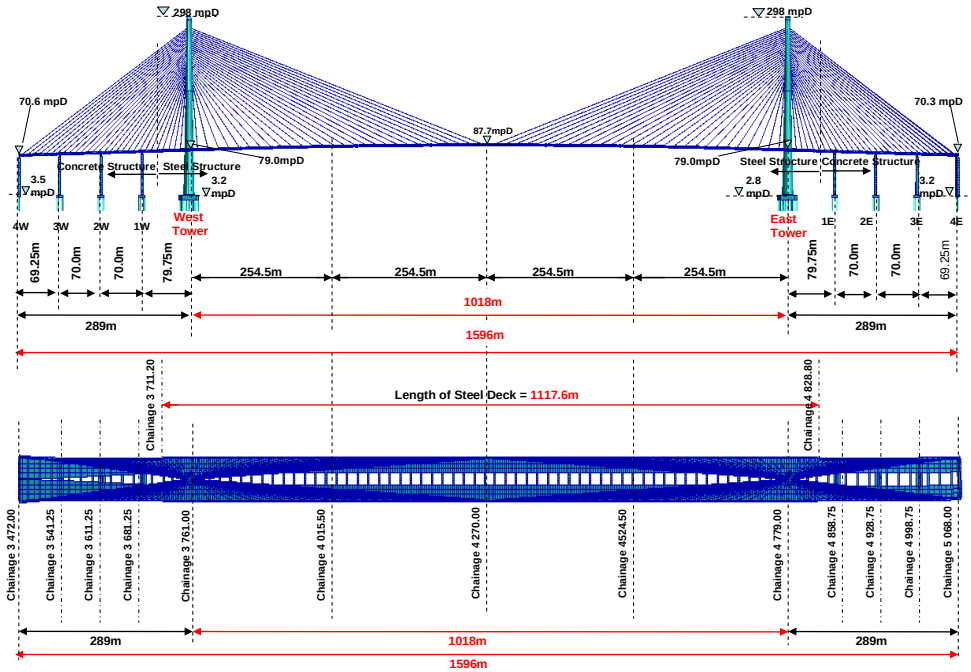

Fig. 16 Structural configuration of Stonecutters Bridge

4.2. Displacement influence line measurement of Stonecutters Bridge

The Stonecutters Bridge in Hong Kong is the third longest spanning cable-stayed bridge in the world with a main span stretching 1,018 m, as shown in Fig. 16. It is a two-cable-plane cable-stayed bridge straddling the Rambler Channel at the entrance to the container terminals and hereby interconnecting the Tsing Yi Island with the Stonecutters Island. One of the most salient structural features of this bridge is the separated and streamlined twin-box girder system at central span consisting of 65 steel deck segments made up of two longitudinal girders connected by rectangular cross beams perpendicular to the longitudinal girders. Additionally, the bridge is supported by two hybrid mono-column pylons which are made up of two distinct portions, i.e., the concrete portion from the pile cap level to a height of 175 m and the steel-concrete composite portion from 175 m to the top of the tower (298 m).

Upon the completion of the bridge construction and before opening to public traffic, traffic loading tests were carried out by the Highways Department of the Hong Kong Special Administrative Region Government to check the structural integrity of the bridge. As illustrated in Fig. 17, the bridge deck was partitioned into 8 traffic lanes and loading trucks with a weight of 42 tons each were mobilized to travel along the bridge deck with specified speeds during the loading tests. An LED lamp target was attached on a deck parapet near Lane 1 at the mid-span of the Stonecutters Bridge and the digital camera was placed on the ground level at the Tsing Yi Island. The estimated distance between the digital camera and the LED lamp target is 500 m. The vertical displacement responses of the Stonecutters Bridge at mid-span were measured by the vision-based system at a sampling frequency of 5 Hz for different loading test scenarios.

Fig. 18 illustrates the vertical displacement influence lines of the Stonecutters Bridge at mid-span measured by the vision-based system when one loading truck separately travels on Lanes 1, 3, 5, and 7, respectively, with a speed of 15 km/h. It is seen from Fig. 18 that the displacement responses increase when the loading truck approaches the mid-span location and decrease when it departs from the mid-span. The maximum amplitude of the measured vertical displacement of the Stonecutters Bridge at mid-span is 56.46 mm, 48.40 mm, 38.10 mm, and 29.07 mm, respectively, in the afore-mentioned loading test scenarios. Fig. 19 illustrates the measured vertical displacement influence lines of the Stonecutters Bridge at mid-span when two loading trucks travel simultaneously on two adjacent lanes along the bridge deck at a speed of 15 km/h. It is seen from Fig. 19 that the maximum amplitude of the measured vertical displacement of the Stonecutters Bridge at mid-span is 106.40 mm, 93.17 mm, 71.01 mm, and 56.40 mm when two loading trucks travel simultaneously on Lanes 1 and 2, Lanes 3 and 4, Lanes 5 and 6, and Lanes 7 and 8, respectively.

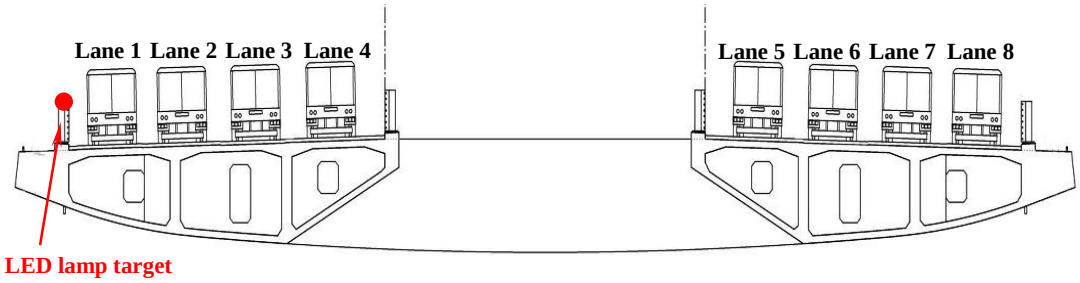

Fig. 17 Traffic lane distribution of Stonecutters Bridge during loading tests

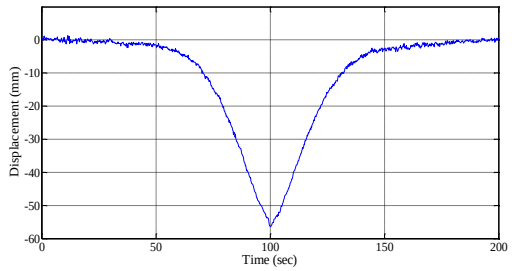

(a) Lane 1

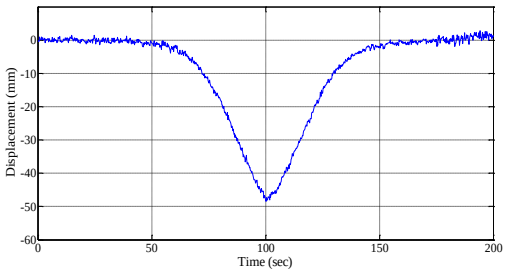

(b) Lane 3

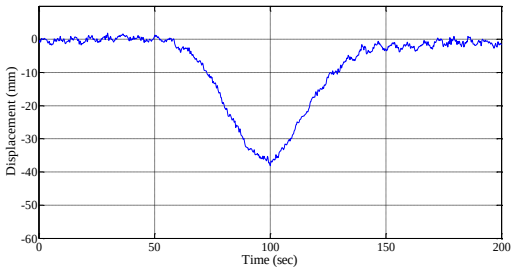

(c) Lane 5

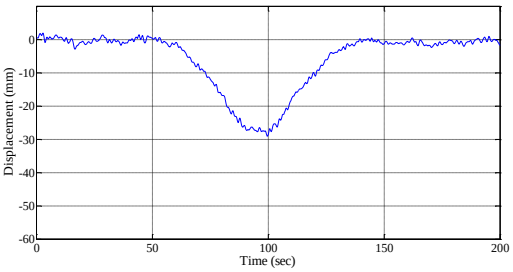

(d) Lane 7

Fig. 18 Measured vertical displacement influence lines of Stonecutters Bridge at mid-span in one-truck scenarios

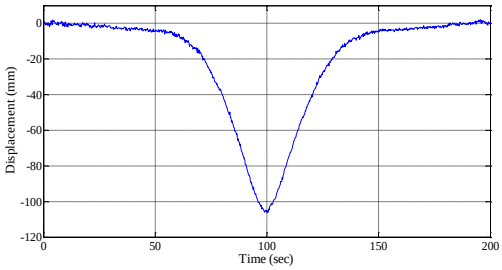

(a) Lanes 1 and 2

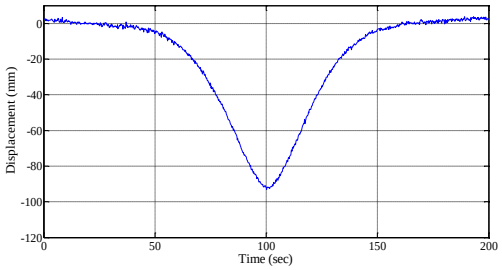

(b) Lanes 3 and 4

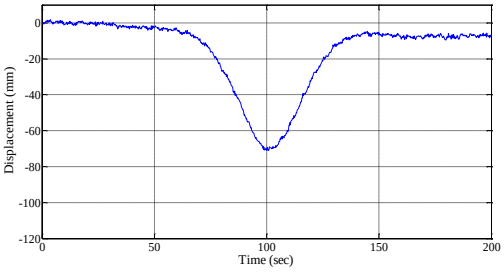

(c) Lanes 5 and 6

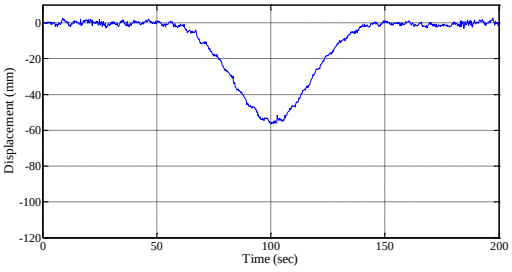

(d) Lanes 7 and 8

Fig. 19 Measured vertical displacement influence lines of Stonecutters Bridge at mid-span in two-truck scenarios

5. Conclusions

This study presented the methodology and experimental verification of a vision-based system for dynamic displacement measurement of long-span bridges. An image acquisition device comprising an advanced industrial CCD digital camera integrated with an extended-range zoon lens has been developed, which is capable of capturing the digital images of a target on the structure over one thousand meters away. The structural displacement was measured in real time through continuously performing the pattern matching process between the predefined pattern and the succeeding images captured by the digital camera. The performance of the developed vision-based system was evaluated by laboratory MTS and shaking table tests. In the MTS tests of sinusoidal motions, the displacements of different types of target (the LED lamp target and the black dot target) measured by the vision-based system were compared with those from the MTS under different vibration frequencies and amplitudes, and a good agreement was observed. The shaking table tests of a single-story steel frame model under different excitations (the El-Centro earthquake wave and a sinusoidal motion of 0.9 Hz) revealed that the displacement responses measured by the vision-based system coincided well with those measured by a laser transducer in both the time and frequency domains. In the field experiments of measuring the mid-span vertical structural displacement of the Tsing Ma Bridge in the operational condition, the developed vision-based system showed its robust capability of long-distance remote displacement measurement. A good agreement between the measured vertical displacements of the Tsing Ma Bridge by the vision-based system and those measured by the GPS was obtained. The developed vision-based system also has been successfully applied in the measurement of vertical displacement influence lines of the Stonecutters Bridge at mid-span under different loading scenarios. Based on the laboratory and field experimental results, it is concluded that the developed vision-based system enables non-contact, long-distance, and high-precision structural dynamic displacement measurement for large-scale bridges. This system is viable especially when the contact-type displacement measurement solutions are impossible or very difficult.

Acknowledgments

The work described in this paper was supported by The Hong Kong Polytechnic University under the grants G-YK83 and G-YM25. The writers also wish to thank the engineers at the Highways Department of the Hong Kong SAR Government for their support throughout the work.

References

Chang, C.C. and Ji, Y.F. (2007), "Flexible videogrammetric technique for three-dimensional structural vibration measurement", *J. Eng. Mech. - ASCE*, **133**(6), 656-664.

Choi, H.S., Cheung, J.H., Kim, S.H. and Ahn, J.H. (2011), "Structural dynamic displacement vision system using digital image processing", *NDT& E. Int.*, **44**(7), 597-608.

Fukuda, Y., Feng, M.Q. and Shinozuka, M. (2010), "Cost-effective vision-based system for monitoring dynamic response of civil engineering structures", *Struct. Health Monit.*, **17**(8), 918-936.

Gonzalez, R.C. and Woods, R.E. (2008), *Digital image processing*, 3rd Ed, Pearson Prentice Hall, Upper Saddle River, NJ.

Jauregui, D.V., White, K.R., Woodward, C.B. and Leitch, K.R. (2003), "Noncontact photogrammetric measurement of vertical bridge deflection", *J. Bridge Eng. - ASCE*, **8**(4), 212-222.
Jurjo, D.L.B.R., Magluta, C., Roitman, N. and Goncalves, P.B. (2010), "Experimental methodology for the dynamic analysis of slender structures based on digital image processing techniques", *Mech. Syst. Signal Pr.*, **24**(5), 1369-1382.
Kim, N.S. and Cho, N.S. (2004), "Estimating deflection of a simple beam model using fiber optic Bragg-grating sensors", *Exp. Mech.*, **44**(4), 433-439.
Kim, W. and Laman, J.A. (2012), "Seven-year field monitoring of four integral abutment bridges", *J. Perform. Constr. Fac. - ASCE*, **26**(1), 54-64.
Ko, J.M. and Ni, Y.Q. (2005), "Technology developments in structural health monitoring of large-scale bridges", *Eng. Struct.*, **27**(12), 1715-1725.
Lee, J.J. and Shinozuka, M. (2006), "A vision-based system for remote sensing of bridge displacement", *NDT& E. Int.*, **39**(5), 425-431.
Nassif, H.H., Gindy, M. and Davis, J. (2005), "Comparison of laser Doppler vibrometer with contact sensors for monitoring bridge deflection and vibration", *NDT&E. Int.*, **38**(3), 213-218.
Ni, Y.Q., Xia, Y., Liao, W.Y. and Ko, J.M. (2009), "Technology innovation in developing the structural health monitoring system for Guangzhou New TV Tower", *Struct. Health Monit.*, **16**(1), 73-98.
Okasha, N.M. and Frangopol, D.M. (2012), "Integration of structural health monitoring in a system performance based life-cycle bridge management framework", *Struct. Infrastruct. E.*, **8**(11), 999-1016.
Park, K.T., Kim, S.H., Park, H.S. and Lee, K.W. (2005), "The determination of bridge displacement using measured acceleration", *Eng. Struct.*, **27**(3), 371-378.
Santos, C.A., Costa, C.O. and Batista, J.P. (2012), "Calibration methodology of a vision system for measuring the displacements of long-deck suspension bridges", *Struct. Health Monit.*, **19**(3), 385-404.
Stull, C.J., Hemez, F.M. and Farrar, C.R. (2012), "On assessing the robustness of structural health monitoring technologies", *Struct. Health Monit.*, **11**(6), 712-723.
Wahbeh, A.M., Caffrey, J.P. and Masri, S.F. (2003), "A vision-based approach for the direct measurement of displacements in vibrating systems", *Smart Mater. Struct.*, **12**(5), 785-794.
Wong, K.Y. (2004), "Instrumentation and health monitoring of cable-supported bridges", *Struct. Health Monit.*, **11**(2), 91-124.
Wong, K.Y. (2007), "Design of a structural health monitoring system for long-span bridges", *Struct. Infrastruct. E.*, **3**(2), 169-185.
Xu, L., Guo, J.J. and Jiang, J.J. (2002), "Time-frequency analysis of a suspension bridge based on GPS", *J. Sound Vib.*, **254**(1), 105-116.
Yi, T.H., Li, H.N. and Gu, M. (2011), "Characterization and extraction of global positioning system multipath signals using improved particle filtering algorithm", *Meas. Sci. Technol.*, **22**(7), Article ID 075101: 1-11.
Yi, T.H., Li, H.N. and Gu, M. (2012). "Recent research and applications of GPS-based monitoring technology for high-rise structures", *Struct. Health Monit.*, DOI: 10.1002/stc.1501.
Yi, T.H., Li, H.N. and Gu, M. (2013), "Experimental assessment of high-rate GPS receivers for deformation monitoring of bridge", *Measurement*, **46**(1), 420-432.
Zaurin, R. and Catbas, F.N. (2010), "Integration of computer imaging and sensor data for structural health monitoring of bridges", *Smart Mater. Struct.*, **19**(1), 1-15.